

1           An abyssal carbonate compensation depth overshoot in the  
2           aftermath of the Paleocene-Eocene Thermal Maximum

3  
4                   Donald E. Penman  
5                   Sandra Kirtland Turner  
6                   Philip F. Sexton  
7                   Richard D. Norris  
8                   Alexander J. Dickson  
9                   Slah Boulila  
10                  Andy Ridgwell  
11                  Richard E. Zeebe  
12                  James C. Zachos  
13                  Adele Cameron  
14                  Thomas Westerhold  
15                  Ursula Röhl  
16  
17

18   **During the Paleocene-Eocene Thermal Maximum (PETM) about 56 million years**  
19 **ago, thousands of petagrams of carbon were released into the atmosphere and ocean**  
20 **in just a few thousand years, followed by a gradual sequestration over**  
21 **approximately 200,000 years. If silicate weathering is one of the key negative**  
22 **feedbacks that removed this carbon, a period of seawater calcium carbonate**  
23 **saturation greater than pre-event levels is expected during the event's recovery**  
24 **phase. In marine sediments, this could be recorded as a temporary deepening of the**  
25 **depth below which no calcite is preserved - the calcite compensation depth (CCD).**  
26 **Previous and new sedimentary records from sites that were above the pre-PETM**  
27 **calcite compensation depth show enhanced carbonate accumulation following the**  
28 **PETM. A new record from an abyssal site in the North Atlantic that lies below the**  
29 **pre-PETM calcite compensation depth shows a period of carbonate preservation**  
30 **beginning about 70,000 years after the onset of the PETM, providing the first direct**  
31 **evidence for an over-deepening of the calcite compensation depth. This record**  
32 **confirms an overshoot in ocean carbonate saturation during the PETM recovery.**

33 **Simulations with two earth system models support scenarios for the PETM that**  
34 **involve both a large initial carbon release followed by prolonged low-level emissions,**  
35 **consistent with the timing of CCD deepening in our record. Sequestration of these**  
36 **emissions was most likely the result of both globally enhanced calcite burial above**  
37 **the calcite compensation depth and, at least in the North Atlantic, by a temporary**  
38 **over-deepening of the calcite compensation depth.**

39

40 The Paleocene-Eocene Thermal Maximum (PETM; ~56 Ma) represents one of the  
41 largest and most abrupt greenhouse warming events in Earth history. Marine and  
42 terrestrial records document a global  $>2.5\%$  negative carbon isotope excursion (CIE)<sup>1-3</sup>  
43 coincident with global mean surface ocean warming of  $>4^{\circ}\text{C}$ <sup>4</sup> and geochemical and  
44 sedimentological evidence for ocean acidification<sup>5,6</sup>. Collectively, these lines of evidence  
45 suggest a rapid ( $10^3$ - $10^4$  years) and massive (~3,000-10,000 PgC) release of  $^{13}\text{C}$ -depleted  
46 carbon into the ocean-atmosphere system<sup>7-9</sup>. The PETM thus offers the opportunity to  
47 examine the response and recovery of the global carbon cycle and seawater carbonate  
48 chemistry to an ancient  $\text{CO}_2$  release similar in magnitude to ongoing anthropogenic fossil  
49 fuel combustion<sup>10</sup>.

50 Current understanding of long-term carbon cycle processes predicts that rapid  
51 carbon injection should cause a short-term ( $0$ - $10^4$  years) period of ocean acidification  
52 featuring reduced seawater carbonate saturation ( $\Omega$ ), followed by a longer-term ( $10^4$ -  
53  $10^5$ .years) period of carbonate oversaturation due to elevated terrestrial silicate  
54 weathering rates (see Box 1). This carbonate saturation overshoot manifests itself in  
55 several carbon cycle model simulations of the PETM<sup>9,11</sup> as an over-deepening of the CCD

56 relative to its pre-event depth. Yet no records exist from abyssal sites below the pre-  
57 PETM CCD with which to detect possible CCD over-deepening. Sedimentary records  
58 from above the CCD (Southern Ocean Site 690<sup>12-15</sup> at ~1900m paleodepth and South  
59 Atlantic Sites 1263<sup>5,14,15</sup> at ~1500m paleodepth and 1266<sup>5,16</sup> at ~2500m paleodepth) show  
60 increases in CaCO<sub>3</sub> content and accumulation rate during and after the PETM recovery<sup>13-</sup>  
61 <sup>15</sup>. These supra-CCD records are consistent with weathering feedbacks prompting  
62 increased carbonate burial during the PETM recovery, and provide important constraints  
63 because the long-term requirement to balance the elevated weathering flux only requires  
64 carbonate burial to increase globally (not necessarily buried at deeper depths). It is thus  
65 theoretically possible to accommodate such elevated global carbonate burial without  
66 substantial deepening of the CCD<sup>17</sup>. Nonetheless, some models<sup>9-11</sup> predict that a testable  
67 facet of the recovery process from massive carbon cycle perturbation involves an over-  
68 deepening of the CCD, and the location of these sites above the pre-PETM CCD means  
69 that they cannot directly test for this predicted CCD over-deepening. Direct observational  
70 evidence from sites sufficiently deep to test for a post-PETM CCD overshoot has thus far  
71 remained elusive.

## 72 **New records from the North Atlantic**

73 Here we present lithology, CaCO<sub>3</sub> content, and carbon isotope ( $\delta^{13}\text{C}$ ) records  
74 from recently recovered sediment cores in the North Atlantic (IODP Sites U1403, PETM  
75 paleodepth ~4374m and U1409, paleodepth ~2913m<sup>18</sup>) that provide important constraints  
76 on the evolution of the CCD through the PETM, including the first evidence for CCD  
77 over-deepening during the PETM recovery. To explore the broader implications of these  
78 records for PETM carbon emissions scenarios, we present new carbon release

79 experiments using two carbon cycle models – LOSCAR<sup>9,19</sup> and cGENIE<sup>20,21</sup> and discuss  
80 uncertainties in the representation of geological carbon cycling in current models.

81 At Site U1409, the PETM CIE occurs in an interval of variously silicified  
82 sediments (siliceous claystones, siliceous limestones and cherts) at 178.9-179.2 mcd  
83 (Figure 1A), contrasting with the nannofossil chalk that characterizes much of the  
84 Paleogene at this site<sup>18</sup>. Although likely somewhat condensed, the  $\delta^{13}\text{C}_{\text{carb}}$  record bears  
85 the typical<sup>15</sup> PETM CIE pattern of an abrupt decrease (here of  $\sim 2\text{‰}$ ) followed by a  
86 plateau of low values and then gradual recovery (Fig. 1). Bulk  $\delta^{13}\text{C}_{\text{carb}}$  over the PETM  
87 CIE interval sampled a heterogeneous mixture of lithology (clay, carbonate-rich burrows  
88 within that clay, and siliceous sediments), with all three lithologies revealing significantly  
89 lower  $\delta^{13}\text{C}$  within the CIE than pre-event values. The integrity of the bulk  $\delta^{13}\text{C}_{\text{carb}}$  record  
90 is also supported by the close structural similarity between it and the equivalent bulk  
91  $\delta^{13}\text{C}_{\text{carb}}$  records from the Southern Ocean and Walvis Ridge (Fig. 1, 2A). The Site U1409  
92  $\delta^{13}\text{C}$  record from benthic foraminifera is discontinuous owing to silicification across the  
93 onset and initial recovery, but minimum values within the CIE show a large ( $\sim 3\text{‰}$ )  
94 excursion, similar to that seen in benthic records from the Southern Ocean<sup>22</sup> and South  
95 Atlantic<sup>23</sup>. Below the CIE, carbonate content is between 60-70 wt%, decreases to a  
96 minimum of  $\sim 40$  wt% at the CIE onset, and rebounds to  $\sim 70\%$  following the CIE. This  
97 pattern is similar to other pelagic PETM sections<sup>24</sup> and implies that the local CCD was  
98 always deeper than the paleodepth of Site U1409, while the decrease in carbonate during  
99 the PETM can be interpreted as a transient decrease in the calcite saturation state,  $\Omega$ ,  
100 consistent with shoaling of the CCD. The absence of near-0 wt%  $\text{CaCO}_3$  sediment at Site  
101 U1409 contrasts with records from the South Atlantic Ocean<sup>5</sup> where cores even shallower

102 than U1409 are barren of carbonate within the CIE. Although this observation could  
103 imply that CCD shoaling in the North Atlantic was less dramatic than that in the South  
104 Atlantic, hiatuses, bioturbation by burrowing, or incomplete recovery of this silicified  
105 interval could have obscured or resulted in the loss of the interval containing the lowest  
106 wt% CaCO<sub>3</sub> values. Regardless, carbonate content and accumulation rate at Site U1409  
107 were higher during the PETM recovery than before the event, similar to other sites at  
108 mid-ocean depths or shallower<sup>5,12-14,16</sup>, thus providing support for elevated saturation  
109 states and increased carbonate burial above the CCD during the recovery phase.

110 Lower abyssal Site U1403 features a prominent transition (over ~5 cm) from  
111 carbonate-poor (<0.5 wt%) claystone in the Upper Paleocene (extending from the P-E  
112 boundary to at least ~61 Ma<sup>18</sup>) to carbonate-bearing (~20-30 wt%) nannofossil claystone  
113 in the lower Eocene (Figure 1B). This carbonate-rich interval contains calcareous  
114 nannofossils of zone NP9B, including PETM excursion taxa *Discoaster araneus* and  
115 *Rhomboaster* spp<sup>18</sup>. Bulk  $\delta^{13}\text{C}_{\text{org}}$  reveals a negative CIE between 200.7 and 201.5 mcd  
116 that is superimposed on comparatively high amplitude orbital timescale variability in the  
117 late Paleocene. The  $\delta^{13}\text{C}_{\text{carb}}$  record necessarily begins at the onset of carbonate  
118 sedimentation with low values of ~0.6‰, followed by a gradual 1.4‰ increase over the  
119 next ~1.6 m, parallel to the recovery in  $\delta^{13}\text{C}_{\text{org}}$ . Given the simultaneous trends to higher  
120 values in both  $\delta^{13}\text{C}_{\text{carb}}$  and  $\delta^{13}\text{C}_{\text{org}}$  within zone NP9B, this  $\delta^{13}\text{C}$  increase can be  
121 unambiguously assigned to the PETM CIE recovery. The magnitude of the  $\delta^{13}\text{C}_{\text{carb}}$   
122 increase (1.4‰) is close to the full amplitude of the PETM CIE recovery observed in  
123 bulk carbonates globally<sup>15</sup> and at Site U1409 (Figure 2A), so we confidently assign the  
124 onset of carbonate sedimentation at Site U1403 to early in the PETM recovery phase.

125 We construct age models by correlating the  $\delta^{13}\text{C}_{\text{carb}}$  records to a compilation of  
126 bulk and fine-fraction  $\delta^{13}\text{C}_{\text{carb}}$  on an orbitally calibrated age model<sup>15</sup> (Figure 2A and 2C).  
127 This age model, based on several PETM sites, produces a shorter duration of the PETM  
128 CIE than extraterrestrial  $^3\text{He}$ -based estimates,<sup>12,16</sup> so durations here may represent  
129 minima. On this timescale, carbonate sedimentation begins at Site U1403 ~70kyr after  
130 the PETM onset and is followed by a period of elevated (20-40) wt%  $\text{CaCO}_3$  that persists  
131 for a further ~150kyr. Fluctuations between 5 and 25 wt%  $\text{CaCO}_3$  continue throughout  
132 the lower Eocene. Although the CIE onset at Site U1403 (as defined by the somewhat  
133 noisy  $\delta^{13}\text{C}_{\text{org}}$  record) introduces some uncertainty around the placement of the P-E  
134 boundary, this does not affect the relative timing of the initial appearance of carbonate at  
135 this lower abyssal site, which is unambiguously assigned to the PETM recovery interval  
136 based on  $\delta^{13}\text{C}_{\text{carb}}$  and the occurrence of PETM excursion-interval calcareous  
137 nannofossils.

138 The pattern of carbonate sedimentation at Site U1403 (carbonate-barren in the  
139 Paleocene with carbonate appearing during the PETM recovery) has not previously been  
140 observed in sediments spanning the PETM. The absence of carbonate in the Upper  
141 Paleocene and into the earliest Eocene indicates the CCD lay shallower than Site U1403  
142 before the PETM and through the CIE onset and body. The onset of carbonate  
143 sedimentation ~70kyr after the PETM onset indicates that the CCD over-deepened to  
144 below the ~4400 m lower abyssal paleo-water depth of Site U1403 during the early phase  
145 of PETM recovery – direct evidence for a post-PETM CCD overshoot. The ~150kyr  
146 period of elevated carbonate deposition at Site U1403 represents the main phase of the  
147 CCD over-deepening, and is coeval with enhanced carbonate accumulation and

148 preservation at shallower paleodepths documented here at Site U1409 and  
149 elsewhere<sup>5,13,14,16</sup> (Figure 2D). These observations strongly implicate elevated whole-  
150 ocean saturation state as the cause of enhanced carbonate burial at all water depths and  
151 from the North Atlantic to the Southern Ocean.

### 152 **Implications of a CCD overshoot explored with carbon cycle models**

153 To explore the implications of a CCD overshoot and its timing, and the CCD  
154 over-deepening at U1403 in particular, we tested a variety of PETM carbon emissions  
155 scenarios using the models LOSCAR and cGENIE. Rather than carry out an extensive  
156 sweep of all combinations of plausible size and duration of carbon release, our emissions  
157 scenarios are based on ref. <sup>9</sup>, characterized by an initial C input ( $\delta^{13}\text{C} = -50\text{‰}$ ) of 3000  
158 PgC over 5 kyr, followed by 1480 PgC over 50 kyr, and originally developed to best  
159 match records of carbonate dissolution (particularly in the South Atlantic<sup>5</sup>). However, we  
160 explored a number of variations on this basic emissions trajectory (Figs. S4-S15) such as  
161 doubling the total mass with half the isotopic composition ( $\delta^{13}\text{C} = -25\text{‰}$ ). In order to  
162 isolate the response of carbonate burial dynamics from circulation effects that might  
163 diverge in the two models, we ran cGENIE with radiative forcing (and thus ocean  
164 circulation) fixed, and for direct comparison with cGENIE (Figure 3) we omitted the  
165 prescribed circulation changes of ref. 9 in LOSCAR. We tracked the evolution of global  
166 sedimentary wt%  $\text{CaCO}_3$  preserved, and simulated the expected marine sediment record  
167 in modeled ‘cores’ at North Atlantic depths approximating Sites U1409 and U1403.

168 The configurations of both LOSCAR and cGENIE models used here include a  
169  $\text{CO}_2$ -dependent silicate weathering feedback (see methods). Both models simulate a  
170 global CCD and wt%  $\text{CaCO}_3$  overshoot which occurs between 20 and 45 kyr after the

171 onset of carbon emissions and peaks between 65 and 97 kyr after the onset, depending on  
172 the emissions schedule and model (Figure 3 and Figure S3)<sup>9,11</sup>. The carbonate overshoot  
173 begins earlier when the carbon pulse occurs over a shorter interval of time (Figures S6,  
174 S12). The long delay (~70kyr) in the onset of carbonate sedimentation at Site U1403 that  
175 we infer from our age model is hence difficult to reconcile with only a short “spike” of  
176 carbon released at the onset of the PETM. Rather, the delay is better explained by a  
177 sustained release of carbon lasting many tens of kyr after an initial spike (Figure 3, S1),  
178 consistent with the conclusions of refs. <sup>9</sup> and <sup>6</sup>. Such sustained carbon release might arise  
179 as a feedback response to initial warming<sup>25,26</sup> or represent prolonged North Atlantic  
180 volcanism. Our experiments also demonstrate that the timing of the overshoot is not  
181 particularly sensitive to the mass of carbon released – doubling the mass of carbon results  
182 in < 2 kyr delay in overshoot timing (e.g. Figure S4 vs. Figure S5).

183         While both models generate a whole-ocean carbonate burial overshoot during the  
184 recovery interval, the spatial distribution of CaCO<sub>3</sub> content in sediments shows  
185 differences both between the models and in comparison to Sites U1403 and U1409  
186 (Figure 3). Because LOSCAR has much coarser spatial resolution (e.g. it represents the  
187 deep Atlantic as a single box), regional patterns need to be interpreted with greater  
188 caution. Nevertheless, LOSCAR generates a deep (4500m) %CaCO<sub>3</sub> overshoot  
189 comparable to that seen at Site U1403, but in shallow sediments (3000m) generates a  
190 larger %CaCO<sub>3</sub> decrease (to near-zero) and smaller overshoot than seen at Site U1409. In  
191 contrast, cGENIE closely matches the Site U1409 record, but at 5000m, sediments  
192 overshoot their pre-event %CaCO<sub>3</sub> levels by only ~1%. It appears that in response to  
193 enhanced weathering-driven elevated saturation states, LOSCAR accommodates greater

194 global carbonate burial with higher %CaCO<sub>3</sub> in deep sediments (an over-deepening of the  
195 CCD), whereas cGENIE accommodates greater global carbonate burial predominantly  
196 within and above the lysocline. Observational evidence (in the form of new and previous  
197 carbonate accumulation rate records) suggest that in the real world (at least in the case of  
198 the PETM), both of these processes may operate.

199         The differences between the models' predictions for the locus of intensified  
200 carbonate burial result from of how the models represent sedimentary processes. In  
201 cGENIE, the respiration of organic carbon in sediments reduces porewater saturation  
202 state and dissolves CaCO<sub>3</sub> even in shallow sediments well above the carbonate saturation  
203 horizon. Because of this, those shallow sediments have greater potential to accommodate  
204 an increase in CaCO<sub>3</sub> content in response to higher bottom water saturation state such as  
205 that seen in the aftermath of the PETM. cGENIE thus balances enhanced weathering flux  
206 via elevated carbonate burial mostly in shallow sediments (within and above the  
207 lysocline)<sup>17</sup>. Conversely, %CaCO<sub>3</sub> in sediments above the lysocline in LOSCAR is set by  
208 the ratio of clay to CaCO<sub>3</sub> in the sediment rain (81% CaCO<sub>3</sub> in the present  
209 configuration)<sup>19</sup>, so when saturation state increases those shallow sediments cannot  
210 accommodate higher CaCO<sub>3</sub> contents (they are already at a maximum). Hence, LOSCAR  
211 balances an increase in weathering flux via enhanced carbonate burial within the  
212 lysocline and below the (pre-event) CCD.

213         A notable aspect of the Site U1403 carbonate record is that following the main  
214 phase of the CCD over-deepening featuring the highest carbonate contents, wt% CaCO<sub>3</sub>  
215 does not return to 0% (its pre-event level) before the next major hyperthermal (ETM-2,  
216 ~2Myr later<sup>18</sup>) (Fig. 1, 2). Hence, the North Atlantic CCD did not return to its pre-PETM

217 state. Two possible explanations exist for this observation. First, negative feedbacks on  
218 carbonate undersaturation could have been very slow to re-establish equilibrium. This is  
219 unlikely, given that all other records of environmental and carbon-cycle perturbation  
220 during the PETM (such as temperature<sup>4</sup>, pH<sup>27</sup>, and the CIE<sup>15</sup>) recovered in hundreds of  
221 thousands of years, not millions. Second, the carbon cycle might have transitioned to a  
222 new equilibrium state featuring a deeper CCD. Several mechanisms may help explain a  
223 deeper post-PETM equilibrium CCD in the North Atlantic. Importantly, the PETM CCD  
224 evolution may have been superimposed on a long-term (multi-million year) global CCD  
225 deepening trend<sup>28-31</sup>. Increasing  $p\text{CO}_2$  on multi-million year timescales across the Late  
226 Paleocene-Early Eocene from greater volcanic  $\text{CO}_2$  release or an imbalance between  
227 terrestrial  $\text{C}_{\text{org}}$  oxidation and marine  $\text{C}_{\text{org}}$  burial could have strengthened weathering rates,  
228 thus increasing seawater carbonate saturation and driving a gradual CCD deepening from  
229 ~58 to ~52Ma, independently of the PETM<sup>28</sup>. Indeed, LOSCAR simulations of carbon  
230 release superimposed on gradual long-term CCD deepening (Figure S2) agree well with  
231 observations from Site U1403, including the persistence of the overshoot.

232 Changing ocean circulation or regional carbonate export across the PETM might  
233 have also affected the regional North Atlantic CCD (i.e. the observed CCD over-  
234 deepening was not necessarily global). Weakened North Atlantic-sourced overturning  
235 during the acidification phase followed by strengthened overturning during the  
236 oversaturation phase could have produced the initial large CCD shoal documented at  
237 Walvis Ridge<sup>5</sup> (South Atlantic) and the later CCD over-deepening at Site U1403 (North  
238 Atlantic). If such circulation changes persisted for several Myr, they could have produced  
239 a persistently deeper post-PETM North Atlantic CCD. Spatial benthic  $\delta^{13}\text{C}$  gradients can

240 shed light on circulation changes<sup>22</sup>, because the accumulation of respired  $C_{org}$  reduces the  
241  $\delta^{13}C$  of deep water DIC as it ages. Owing to its location in the lower abyss, Site U1403 is  
242 unfortunately nearly barren of benthic foraminifera throughout the PETM and its  
243 recovery. However, Site U1409 benthic  $\delta^{13}C$  values overlap with those of South  
244 Atlantic<sup>23</sup> and Southern Ocean<sup>22</sup> during intervals immediately prior to the PETM and  
245 during the later stages of the recovery, including the time interval (>110kyr after the  
246 event) during which Site U1403 documents a CCD overshoot (Figure 2). Benthic  
247 gradients between the South and North Atlantic therefore do not show any evidence for  
248 large-scale changes in Atlantic overturning circulation during the PETM recovery that  
249 could have contributed to a localized CCD over-deepening.

250         Other processes could have also contributed to CCD over-deepening during the  
251 PETM recovery, specifically those processes that could have removed carbon from the  
252 ocean/atmosphere and increase seawater pH and saturation state (in a sense, the opposite  
253 of the PETM acidification phase), and hence influence the CCD. In particular, studies  
254 have suggested that the pace of the CIE recovery, which is complete within ~150kyr<sup>12,16</sup>,  
255 is too rapid to be explained by enhanced weathering and carbonate burial alone. Instead,  
256 the preferential removal of  $^{12}C$  via enhanced burial of organic carbon ( $C_{org}$ ) has been  
257 proposed to explain the CIE recovery timing<sup>32</sup>. This is consistent with evidence of  
258 increased marine productivity during the PETM from elevated biogenic barium  
259 accumulation rates<sup>33,34</sup> and coccolith Sr/Ca<sup>35</sup>. Our model experiments focus on the long-  
260 term inorganic carbon cycle and silicate weathering and hence cannot exclude a role for  
261 enhanced organic carbon burial.

262           In summary, our finding of a post-PETM CCD overshoot in the North Atlantic  
263 Ocean constitutes the first evidence for post-PETM variations in carbonate burial from  
264 sediments deeper than the pre-PETM CCD. It thus represents an important constraint on  
265 the vertical extent of the CCD's response to carbon release during the PETM and  
266 consequently, the processes responsible for restoring the carbon cycle to steady state. It is  
267 tempting to use this constraint to directly calculate the mass of carbon released during the  
268 PETM because the excess carbonate burial should scale with the mass of carbon released.  
269 However, we recognize that one site does not fully constrain the global extent of the  
270 overshoot, nor its absolute magnitude. Further constraints on the CCD over-deepening  
271 from even deeper water depths and additional ocean basins are therefore an essential  
272 target for future scientific drilling. Additionally, uncertainty in the strength of the silicate  
273 weathering feedback (Figure S2)<sup>36</sup> as well as the potential influences of initial carbon  
274 cycle conditions, circulation changes, C<sub>org</sub> burial, and changing clay flux preclude explicit  
275 calculation of the total carbon release<sup>10</sup>. Indeed, the differing responses of the two  
276 different global carbon cycle models we have tested against the observations underscore  
277 the lack of consensus on how the marine carbonate carbon sink responds in detail (and  
278 particularly in the depth distribution of CaCO<sub>3</sub> burial) to perturbation. Multiple  
279 combinations of mass and rate of carbon release, weathering feedback strength, and C<sub>org</sub>  
280 burial are consistent with the new observations described here. Our findings nevertheless  
281 provide an important constraint on how carbon was sequestered in the aftermath of the  
282 PETM, an event that continues to guide our understanding of Earth system processes and  
283 feedbacks during large-scale carbon cycle perturbations.  
284

285 **Author Contributions:** DEP, SKT, PFS, RDN, and SB conceived the study and  
286 participated in IODP Expedition 342 that recovered and described the sediments used  
287 here. DEP generated carbonate stable isotope analyses in the lab of JCZ, and AJD  
288 generated organic carbon stable isotope and Coulomat %CaCO<sub>3</sub> analyses. XRF scanning  
289 records were generated by SKT at Scripps, and AC, PFS, TW, and UR at MARUM. DEP  
290 and SKT performed the carbon cycle modeling with guidance from REZ and AR. DEP  
291 wrote the manuscript with help from SKT and PFS, and all authors edited the manuscript.

292

293 **Corresponding author:** Correspondence and requests for materials should be addressed  
294 to Donald E. Penman (donald.penman@yale.edu).

295

## 296 **METHODS**

### 297 **Geochemical analyses**

298 During IODP Expedition 342, drilling operations penetrated the P-E boundary at  
299 Sites U1403 (39°56.5997N, 51°48.1998W, 4946m depth) and U1409 (41°17.7501N,  
300 49°13.9996W, 3502m depth). Shipboard investigation described lithology, identified the  
301 approximate positions of the P-E boundary by nannofossil biostratigraphy, and provided  
302 coarse-resolution records of wt% CaCO<sub>3</sub>. The surface of core archive halves spanning the  
303 PETM were scanned at 1-2 cm-resolution at the MARUM – Center for Marine  
304 Environmental Sciences, University of Bremen and at Scripps Institution of  
305 Oceanography using Avaatech X-ray fluorescence (XRF) core scanners. Estimates of the  
306 total abundance of calcium (Ca) and iron (Fe) were obtained by scanning cores at an  
307 energy level of 10kV, current of 500 uA, count time of 20 sec, and measurement area of

308 10 x 12 mm. Estimated wt% CaCO<sub>3</sub> records were generated by regressing shipboard wt%  
309 CaCO<sub>3</sub> measurements<sup>18</sup> against the natural logarithm of XRF-derived Ca/Fe ratios. For  
310 stable isotope analyses, samples were collected at ~5cm resolution from Site U1409 and  
311 10cm resolution from Site U1403, freeze dried, homogenized with mortar and pestle, and  
312 analyzed for  $\delta^{13}\text{C}_{\text{carb}}$  on a ThermoFisher MAT 253 stable isotope mass spectrometer  
313 coupled to a Kiel IV carbonate device using standard dual-inlet techniques (typical long-  
314 term  $\delta^{13}\text{C}_{\text{carb}}$  reproducibility of carbonate standards is  $< \pm 0.05\%$ , 1 S.D.) In addition,  
315 samples from Site U1409 were washed and sieved, and specimens of the benthic  
316 foraminifera *Nuttalides truempyi* were picked from the 150-200 and 212-300 $\mu\text{m}$  size  
317 fraction. Where possible, 3-8 of these specimens from each sample were run using the  
318  $\delta^{13}\text{C}_{\text{carb}}$  methods described above. For  $\delta^{13}\text{C}_{\text{org}}$  analysis of Site U1403, homogenized  
319 sample powders were de-carbonated in 1M HCL and washed in de-ionized water.  $\delta^{13}\text{C}_{\text{org}}$   
320 was measured using a Thermo-Finnegan MAT 253 mass spectrometer coupled to a  
321 Thermo Scientific 2000 HT elemental analyzer via a Conflo IV interface optimized for  
322 the measurement of samples with low organic carbon abundances. Analytical  
323 reproducibility was monitored using analyses of IAEA CH-6 sucrose and was  $< \pm 0.1\%$   
324 (1 S.D). All  $\delta^{13}\text{C}$  data are expressed relative to V-PDB. Additional Site U1403 wt. %  
325 CaCO<sub>3</sub> was measured using a Strohlein Coulomat.

### 326 **Carbon cycle modeling**

327 LOSCAR is a numerically-efficient geochemical box model of the marine carbon  
328 cycle with realistic interaction with sediments, capable of multi-million year simulations  
329 of carbon cycle processes including CCD depth. All runs use Paleogene LOSCAR  
330 setup<sup>19</sup>. Code availability: the C code for the LOSCAR model can be obtained from

331 author REZ upon request (zeebe@hawaii.edu). cGENIE is an intermediate-complexity  
332 Earth system model including a 3-D dynamic ocean model with biogeochemical cycling  
333 of key elements and isotopes and a spatially resolved sediment model capable of  
334 generating virtual sediment cores – synthetic stacks of deep-sea sediments<sup>20,21,37</sup>. We use  
335 the late Paleocene/early Eocene configuration of ref. <sup>38</sup>. For this study, we evaluate virtual  
336 sediment core results from a depth transect in the North Atlantic ranging from 5000-3000  
337 m water depth and at locations corresponding to Expedition 342 sites.

338 Both models include carbonate and silicate weathering feedbacks. In LOSCAR,  
339 weathering is parameterized as  $F_w = F_{eq} * ([CO_2]_{atm} / [CO_2]_{eq})^{N_{Si}}$ , where  $F_{eq}$  and  $[CO_2]_{eq}$   
340 are equilibrium weathering flux and atmospheric  $pCO_2$  at which volcanic carbon  
341 emissions are perfectly balanced by silicate weathering and carbonate burial<sup>19</sup>.  $N_{Si}$  sets  
342 the strength of the silicate weathering feedback (default  $N_{Si} = 0.2$ ). We implement the  
343 same formulation for a  $CO_2$ -dependent carbonate and silicate weathering feedback in  
344 cGENIE using a model for terrestrial rock weathering<sup>39</sup>. Following ref. <sup>40</sup>, we assume  
345 carbonate weathering proportional to the square root of  $[CO_2]_{atm} / [CO_2]_{eq}$  and silicate  
346 weathering proportional to  $[CO_2]_{atm} / [CO_2]_{eq}$  raised to the power of 0.3. We assume a  
347 50:50 split between carbonate and silicate weathering in order to match total carbonate  
348 burial, and balance silicate weathering with volcanic outgassing. We utilize the cGENIE  
349 and LOSCAR models in this study in order to qualitatively demonstrate what  
350 mechanisms are consistent with the new data, not in an attempt to reconstruct exactly a  
351 PETM scenario.

352 **Data:** Accompanying data can be found at [PANGEA web address forthcoming]

353

354 **FIGURE CAPTIONS**

355 **Figure 1:** Lithology and  $\delta^{13}\text{C}$  over the PETM at Sites U1409 (A) and U1403 (B) plotted  
356 against composite depth (mcd). Each panel shows core photo (Site U1403 vertically  
357 compressed), lithologic description, calcareous nannofossil biostratigraphy, wt. %CaCO<sub>3</sub>  
358 estimated by XRF scanning data (black line), and bulk  $\delta^{13}\text{C}_{\text{carb}}$  (blue line). Lithology  
359 codes for Site U1409: NC = nannofossil chalk, CNC = clayey nannofossil chalk, SL =  
360 siliceous limestone, Cl = claystone, SC = siliceous claystone, Ch = chert. Bulk  $\delta^{13}\text{C}_{\text{org}}$   
361 (green line) and wt. % CaCO<sub>3</sub> measured with a Coulomat device (black X's) are also  
362 shown for Site U1403, and benthic foraminifer *Nuttalides truempyi*  $\delta^{13}\text{C}$  (red squares) is  
363 shown for Site U1409. The heterogeneous mixture of clay- and carbonate-rich facies  
364 within the CIE at Site U1409 is interpreted as carbonate-rich burrows within clay-rich  
365 sediments, with both recording low (<0.5‰) bulk  $\delta^{13}\text{C}$ . Depth intervals representing the  
366 Paleocene, CIE, Recovery, and post-PETM based on  $\delta^{13}\text{C}$  stratigraphy are highlighted  
367 with grey, red, orange, and white shaded bars, respectively. PETM phases nomenclature  
368 from ref. 15.

369

370 **Figure 2:** Age models and PETM isotopic and sedimentological records from new and  
371 previous sites. A: Bulk  $\delta^{13}\text{C}_{\text{carb}}$  records from Sites 690<sup>13</sup>, 1263<sup>15</sup>, U1403, and U1409  
372 plotted on the age model used in this study. B: Weight %CaCO<sub>3</sub> of Sites U1403 and  
373 U1409 (this study), 690<sup>13</sup>, and 1263<sup>5</sup>. C: Linear sedimentation rates used in age models  
374 constructed by this study for Sites U1403 and U1409, and Sites 690 and 1263 from Röhl,  
375 et al. <sup>15</sup> D: Carbonate mass accumulation rate calculated from dry bulk density,  
376 sedimentation rates (C), wt. % CaCO<sub>3</sub> (B). E: Comparison of benthic foraminifer  $\delta^{13}\text{C}$

377 from South Atlantic Site 1263,<sup>23</sup> Southern Ocean Site 690,<sup>22</sup> and U1409 demonstrating  
378 small and constant North-South aging gradient during the CCD overshoot. Green bars  
379 indicate silicified intervals at Site U1409 which precluded measurement of benthic  
380 foraminifers. In (B), (D) and (E), the silicified interval of U1409 is marked with a dashed  
381 line to reflect potential hiatuses or incomplete recovery which may have resulted in an  
382 incomplete %CaCO<sub>3</sub> record (see text).

383

384 **Figure 3:** Comparison of LOSCAR and cGENIE C release experiments using the  
385 Emissions scenario of ref. 9 with radiative forcing (and thus circulation) fixed in  
386 cGENIE, and no circulation changes in LOSCAR. Top panel: Emissions scenario. Middle  
387 panel: modeled 3000m sediment core-top %CaCO<sub>3</sub> compared with Site U1409 %CaCO<sub>3</sub>  
388 record. Bottom panel: modeled 4500m (LOSCAR) and 5000m (cGENIE) sediment core-  
389 top %CaCO<sub>3</sub> compared with Site U1403 %CaCO<sub>3</sub> record. In middle and bottom panels,  
390 thin, opaque traces mark pre-event %CaCO<sub>3</sub> for cGENIE and LOSCAR.

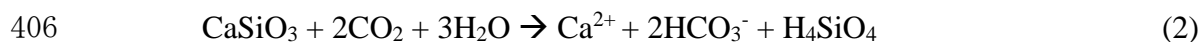
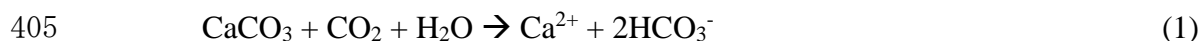
391

### 392 **Box 1: The ocean's two-phase response to rapid carbon injection**

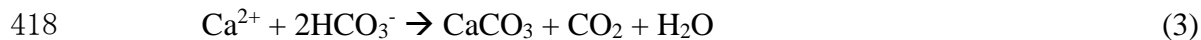
393 Current understanding of long-term carbon cycle processes suggests that large-  
394 scale carbon injection into the ocean-atmosphere should induce a two-phase response in  
395 ocean carbonate saturation. Initially, rapid invasion of CO<sub>2</sub> into the ocean lowers pH and  
396 carbonate saturation state ( $\Omega$ ) in tandem<sup>6,38,41</sup>, resulting in dissolution of both newly  
397 deposited and pre-existing carbonate sediments<sup>5</sup>. The result is a dramatic reduction in  
398 CaCO<sub>3</sub> burial in marine sediments globally and, in places, evidence for a shoaling of the

399 calcite compensation depth (CCD, the depth below which no calcium carbonate, in the  
400 form of calcite, is preserved).<sup>5,24,42</sup>.

401 A second phase of carbonate saturation and burial response arises from elevated  
402 atmospheric pCO<sub>2</sub> and increased global temperatures that are thought to drive an increase  
403 in the rate of terrestrial carbonate and silicate rock chemical weathering<sup>43,44</sup>, which can be  
404 generalized:



407 Accelerating these reactions increases the delivery of Ca<sup>2+</sup> (and thus total alkalinity, TA)  
408 and dissolved inorganic carbon (DIC) to the oceans, elevating Ω. An intensification of  
409 continental weathering during the PETM is supported by a pronounced increase in the  
410 <sup>187</sup>Os/<sup>188</sup>Os of seawater<sup>45,46</sup> and an increase in kaolinite in marine sediments<sup>47</sup>. However,  
411 although the silicate weathering rate responds quickly to increased temperature/CO<sub>2</sub>, the  
412 rate of CO<sub>2</sub> drawdown from global weathering (~ 0.1 PgC/yr<sup>41</sup>) is small in comparison to  
413 estimates of initial carbon release (thousands of PgC)<sup>7-9</sup>, meaning that this feedback  
414 should take >10<sup>4</sup> years to gradually overcome the undersaturation associated with the  
415 initial acidification phase<sup>11,48,49</sup>. On longer timescales (>10<sup>5</sup> years)<sup>49</sup>, this increased  
416 weathering-derived flux of TA and DIC to the oceans must be balanced by carbonate  
417 production and burial to balance the ocean's alkalinity budget:



419 The long-term balance of carbonate weathering with carbonate burial has no permanent  
420 effect on the ocean's TA or DIC budgets (Equation 1 is simply the reverse of Equation 3).  
421 However, the long-term balance of silicate weathering (Equation 2) with carbonate burial

422 (Equation 3) gives rise to a net consumption of CO<sub>2</sub> that is buried as CaCO<sub>3</sub> sediment –  
423 the long-term fate of carbon released during the PETM.

424 The assumption that net CO<sub>2</sub> consumption via elevated silicate weathering and  
425 carbonate burial (Equation 2+3) is responsive to perturbations in climate forms the basis  
426 of a proposed long-term negative (stabilizing) feedback on climate, hypothesized to have  
427 been important in maintaining a habitable climate throughout Earth history<sup>43,44</sup> and  
428 specifically during the PETM recovery<sup>11</sup>. One way in which global carbonate burial could  
429 respond to changing weathering flux is through fluctuations of the global sea-floor area  
430 of carbonate-free sediments (i.e. the CCD). In other words, during the initial acidification  
431 phase, carbonate undersaturation leads to a reduced CaCO<sub>3</sub> sink and a short-term  
432 shoaling of the CCD, whereas on longer timescales (>10<sup>5</sup> years), faster weathering rates  
433 lead to carbonate oversaturation and increased carbonate burial, which might be reflected  
434 in an over-deepening of the CCD<sup>10,11,50</sup>. The interval of excess (compared to pre-PETM)  
435 CaCO<sub>3</sub> burial primarily reflects the removal of carbon released at the onset of the PETM  
436 by enhanced silicate weathering, together with the quantity of CaCO<sub>3</sub> dissolved during  
437 the initial carbonate undersaturation phase and additional terrestrial weathering of  
438 carbonate rocks under warmer temperatures (both of which will be some function of CO<sub>2</sub>  
439 release). The characteristics of any post-PETM CCD overshoot hence potentially hold  
440 key information regarding the magnitude of carbon release and the processes involved in  
441 the recovery from an abrupt carbon cycle perturbation.

442

443

#### References

444

- 445 1 Koch, P. L., Zachos, J. C. & Gingerich, P. D. Correlation Between Isotope  
446 Records in Marine and Continental Carbon Reservoirs Near the Palaeocene  
447 Eocene Boundary. *Nature* **358**, 319-322 (1992).

- 448 2 Kennett, J. P. & Stott, L. D. Abrupt Deep-Sea Warming, Palaeoceanographic  
449 Changes and Benthic Extinctions At the End of the Palaeocene. *Nature* **353**, 225-  
450 229 (1991).
- 451 3 McInerney, F. A. & Wing, S. The Paleocene-Eocene Thermal Maximum: A  
452 Perturbation of Carbon Cycle, Climate, and Biosphere with Implications for the  
453 future. *Annual Review of Earth & Planetary Sciences* **39**, 489-516 (2011).
- 454 4 Dunkley-Jones, T. *et al.* Climate model and proxy data constraints on ocean  
455 warming across the Paleocene-Eocene Thermal Maximum. *Earth-Science*  
456 *Reviews* **125**, 123-145 (2013).
- 457 5 Zachos, J. C. *et al.* Rapid acidification of the ocean during the Paleocene-Eocene  
458 thermal maximum. *Science* **308**, 1611-1615 (2005).
- 459 6 Penman, D. E., Hönisch, B., Zeebe, R. E., Thomas, E. & Zachos, J. C. Rapid and  
460 sustained surface ocean acidification during the Paleocene - Eocene Thermal  
461 Maximum. *Paleoceanography* **29**, 357-369 (2014).
- 462 7 Dickens, G. R., Oneil, J. R., Rea, D. K. & Owen, R. M. Dissociation of Oceanic  
463 Methane Hydrate As a Cause of the Carbon Isotope Excursion At the End of the  
464 Paleocene. *Paleoceanography* **10**, 965-971 (1995).
- 465 8 Panchuk, K., Ridgwell, A. & Kump, L. R. Sedimentary response to Paleocene-  
466 Eocene Thermal Maximum carbon release: A model-data comparison. *Geology*  
467 **36**, 315-318 (2008).
- 468 9 Zeebe, R. E., Zachos, J. C. & Dickens, G. R. Carbon dioxide forcing alone  
469 insufficient to explain Palaeocene-Eocene Thermal Maximum warming. *Nature*  
470 *Geoscience* **2**, 576-580 (2009).
- 471 10 Zeebe, R. & Zachos, J. Long-term legacy of massive carbon input to the Earth  
472 system: Anthropocene vs. Eocene. *Philosophical Transactions of the Royal*  
473 *Society A* **371**, 1-22 (2012).
- 474 11 Dickens, G. R., Castillo, M. M. & Walker, J. C. G. A blast of gas in the latest  
475 Paleocene: Simulating first-order effects of massive dissociation of oceanic  
476 methane hydrate. *Geology* **25**, 259-262 (1997).
- 477 12 Farley, K. A. & Eltgroth, S. F. An alternative age model for the Paleocene-Eocene  
478 thermal maximum using extraterrestrial He-3. *Earth and Planetary Science*  
479 *Letters* **208**, 135-148 (2003).
- 480 13 Kelly, D. C., Zachos, J. C., Bralower, T. J. & Schellenberg, S. A. Enhanced  
481 terrestrial weathering/runoff and surface ocean carbonate production during the  
482 recovery stages of the Paleocene-Eocene thermal maximum. *Paleoceanography*  
483 **20**, PA4023, doi:10.1029/PA001163 (2005).
- 484 14 Kelly, D. C., Nielsen, T. M. J., McCarren, H. K., Zachos, J. C. & Rohl, U.  
485 Spatiotemporal patterns of carbonate sedimentation in the South Atlantic:  
486 Implications for carbon cycling during the Paleocene-Eocene thermal maximum.  
487 *Palaeogeography Palaeoclimatology Palaeoecology* **293**, 30-40 (2010).
- 488 15 Röhl, U., Westerhold, T., Bralower, T. J. & Zachos, J. C. On the duration of the  
489 Paleocene-Eocene thermal maximum (PETM). *Geochemistry Geophysics*  
490 *Geosystems* **8**, Q12002, doi:10.1029/2007GC001784 (2007).
- 491 16 Murphy, B. H., Farley, K. A. & Zachos, J. C. An extraterrestrial He-3-based  
492 timescale for the Paleocene-Eocene thermal maximum (PETM) from Walvis

493 Ridge, IODP Site 1266. *Geochimica Et Cosmochimica Acta* **74**, 5098-5108  
494 (2010).

495 17 Greene, S. *et al.* in *2014 AGU Fall Meeting Abstracts*. PP41C-1407.

496 18 Norris, R. *et al.* Paleogene Newfoundland sediment drifts. *Integrated Ocean*  
497 *Drilling Program: Preliminary Reports*, Exp. 342, 1-263 (2012).

498 19 Zeebe, R. LOSCAR: Long-term ocean-atmosphere-sediment carbon cycle  
499 reservoir model v2. 0.4. *Geoscientific Model Development* **5**, 149-166 (2012).

500 20 Ridgwell, A. & Hargreaves, J. Regulation of atmospheric CO<sub>2</sub> by deep - sea  
501 sediments in an Earth system model. *Global Biogeochemical Cycles* **21**, GB2008,  
502 doi:10.1029/2006GB002764 (2007).

503 21 Ridgwell, A. Interpreting transient carbonate compensation depth changes by  
504 marine sediment core modeling. *Paleoceanography* **22**, PA4102,  
505 doi:10.1029/2006PA001372 (2007).

506 22 Nunes, F. & Norris, R. D. Abrupt reversal in ocean overturning during the  
507 Palaeocene/Eocene warm period. *Nature* **439**, 60-63 (2006).

508 23 McCarren, H., Thomas, E., Röhl, U. & Zachos, J. C. The Paleocene-Eocene  
509 Carbon Isotope Excursion: Insights from the benthic record (ODP Leg 208,  
510 Walvis Ridge). *Geophysics, Geosystems, Geochemistry* **9**, Q10008,  
511 doi:10.1029/GC002116 (2008).

512 24 Zeebe, R. E. & Zachos, J. C. Reversed deep-sea carbonate ion basin gradient  
513 during Paleocene-Eocene thermal maximum. *Paleoceanography* **22**, PA3201.  
514 doi:10.1029/2006PA001395 (2007).

515 25 Zeebe, R. E. What caused the long duration of the Paleocene - Eocene Thermal  
516 Maximum? *Paleoceanography* **26**, 1-13 (2013).

517 26 Bowen, G. J. Up in smoke: A role for organic carbon feedbacks in Paleogene  
518 hyperthermals. *Global and Planetary Change* **109**, 18-29 (2013).

519 27 Penman, D. E., Hönisch, B., Zeebe, R. E., Thomas, E. & Zachos, J. C. Rapid and  
520 sustained surface ocean acidification during the Paleocene - Eocene Thermal  
521 Maximum. *Paleoceanography* **29**, 357-369 (2014).

522 28 Komar, N., Zeebe, R. & Dickens, G. Understanding long - term carbon cycle  
523 trends: The late Paleocene through the early Eocene. *Paleoceanography* **28**, 650-  
524 662 (2013).

525 29 Leon-Rodriguez, L. & Dickens, G. R. Constraints on ocean acidification  
526 associated with rapid and massive carbon injections: The early Paleogene record  
527 at ocean drilling program site 1215, equatorial Pacific Ocean. *Palaeogeography,*  
528 *Palaeoclimatology, Palaeoecology* **298**, 409-420 (2010).

529 30 Hancock, H. J., Dickens, G. R., Thomas, E. & Blake, K. L. Reappraisal of early  
530 Paleogene CCD curves: foraminiferal assemblages and stable carbon isotopes  
531 across the carbonate facies of Perth Abyssal Plain. *International Journal of Earth*  
532 *Sciences* **96**, 925-946 (2007).

533 31 Slotnick, B. *et al.* Early Paleogene variations in the calcite compensation depth:  
534 new constraints using old boreholes across Ninetyeast Ridge in the Indian Ocean.  
535 *Climate of the Past Discussions* **10**, 3163-3221 (2014).

536 32 Bowen, G. J. & Zachos, J. C. Rapid carbon sequestration at the termination of the  
537 Palaeocene-Eocene Thermal Maximum. *Nature Geoscience* **3**, 866-869 (2010).

- 538 33 Bains, S., Norris, R. D., Corfield, R. M. & Faul, K. L. Termination of global  
539 warmth at the Palaeocene/Eocene boundary through productivity feedback.  
540 *Nature* **407**, 171-174 (2000).
- 541 34 Ma, Z. *et al.* Carbon sequestration during the Palaeocene-Eocene Thermal  
542 Maximum by an efficient biological pump. *Nature Geoscience* **7**, 382-388 (2014).
- 543 35 Stoll, H. M. & Bains, S. Coccolith Sr/Ca records of productivity during the  
544 Paleocene-Eocene thermal maximum from the Weddell Sea. *Paleoceanography*  
545 **18**, 1049, doi:10.1029/2002PA00875 (2003).
- 546 36 Uchikawa, J. & Zeebe, R. E. Influence of terrestrial weathering on ocean  
547 acidification and the next glacial inception. *Geophysical Research Letters* **35**,  
548 L23608, doi:10.1029/2008GL035963 (2008).
- 549 37 Ridgwell, A. Application of sediment core modelling to interpreting the glacial-  
550 interglacial record of Southern Ocean silica cycling. *Climate of the Past* **3**, 387-  
551 396 (2007).
- 552 38 Ridgwell, A. & Schmidt, D. N. Past Constraints on the vulnerability of marine  
553 calcifiers to massive carbon dioxide release. *Nature Geoscience* **3**, 196-200  
554 (2010).
- 555 39 Colbourn, G., Ridgwell, A. & Lenton, T. The Rock Geochemical Model  
556 (RokGeM) v0. 9. *Geoscientific Model Development* **6**, 1543-1573 (2013).
- 557 40 Walker, J. C. G. & Kasting, J. F. Effects of fuel and forest conservation on future  
558 levels of atmospheric carbon dioxide. *Palaeogeogr., Palaeoclimatol., Palaeoecol.*  
559 **97**, 151-189 (1992).
- 560 41 Hönisch, B. *et al.* The Geological Record of Ocean Acidification. *Science* **335**,  
561 1058-1063 (2012).
- 562 42 Sluijs, A., Zachos, J. C. & Zeebe, R. E. Constraints on hyperthermals. *Nature*  
563 *Geoscience* **5**, 231-231 (2012).
- 564 43 Walker, J. C. G., Hays, P. B. & Kasting, J. F. A Negative Feedback Mechanism for  
565 the Long-Term Stabilization of Earths Surface-Temperature. *J Geophys Res-Oc*  
566 *Atm* **86**, 9776-9782 (1981).
- 567 44 Berner, R. A., Lasaga, A. C. & Garrels, R. M. The carbonate-silicate geochemical  
568 cycle and its effects on atmospheric carbon dioxide over the past 100 million  
569 years. *American Journal of Science* **283**, 641-683 (1983).
- 570 45 Dickson, A. J. *et al.* Evidence for weathering and volcanism during the PETM  
571 from Arctic Ocean and Peri-Tethys osmium isotope records. *Palaeogeography*  
572 *Palaeoclimatology Palaeoecology* **438**, 300-307.
- 573 46 Ravizza, G., Norris, R. N., Blusztajn, J. & Aubry, M. P. An osmium isotope  
574 excursion associated with the late Paleocene thermal maximum: Evidence of  
575 intensified chemical weathering. *Paleoceanography* **16**, 155-163 (2001).
- 576 47 Robert, C. & Kennett, J. P. Antarctic Subtropical Humid Episode At the  
577 Paleocene-Eocene Boundary - Clay-Mineral Evidence. *Geology* **22**, 211-214  
578 (1994).
- 579 48 Goodwin, P. & Ridgwell, A. Ocean - atmosphere partitioning of anthropogenic  
580 carbon dioxide on multimillennial timescales. *Global Biogeochemical Cycles* **24**,  
581 GB2014, doi:10.1029/2008GB003449 (2010).

- 582 49 Lord, N., Ridgwell, A., Thorne, M. & Lunt, D. An impulse response function for  
583 the “long tail” of excess atmospheric CO<sub>2</sub> in an Earth system model. *Global*  
584 *Biogeochemical Cycles* **30**, 2-17 (2015).
- 585 50 Palike, H., Lyle, M., Nishi, H. & al., e. A Cenozoic record of the equatorial Pacific  
586 carbonate compensation depth. *Nature* **488**, 609-614 (2012).

587  
588  
589

590 **Acknowledgements:** We thank the scientists and crew of IODP Expedition 342 and the  
591 IODP Bremen Core Repository (BCR). We thank M. Gilmour and S. Nicoara for  
592 assistance in the stable isotope laboratory at The Open University, V. Lukies for  
593 assistance in the XRF Core Scanning laboratory at MARUM, University of Bremen ,and  
594 D. Andreasen for assistance with carbonate stable isotope analyses at UC Santa Cruz. The  
595 comments of two anonymous reviewers greatly improved the manuscript. This work was  
596 supported by NSF OCE-1220615 to JZ and RZ and the *Deutsche*  
597 *Forschungsgemeinschaft* (DFG) to UR and TW.

598